PHYSICAL REVIEW B **92**, 041102(R) (2015)

Surface polarization and edge charges

Yuanjun Zhou, Karin M. Rabe, and David Vanderbilt
Department of Physics and Astronomy, Rutgers University, Piscataway, New Jersey 08854, USA
(Received 29 April 2015; published 6 July 2015)

The term "surface polarization" is introduced to describe the in-plane polarization existing at the surface of an insulating crystal when the in-plane surface inversion symmetry is broken. Here, the surface polarization is formulated in terms of a Berry phase, with the hybrid Wannier representation providing a natural basis for study of this effect. Tight-binding models are used to demonstrate how the surface polarization reveals itself via the accumulation of charges at the corners and edges for a two dimensional rectangular lattice and for GaAs respectively.

DOI: 10.1103/PhysRevB.92.041102 PACS number(s): 77.22.Ej, 71.15.−m, 73.20.−r

For over two decades, it has been understood that the electric polarization $\mathbf{P}$ of an insulating crystal is a bulk quantity whose electronic contribution is determined modulo $2e\mathbf{R}/\Omega$ (where $\mathbf{R}$ is a lattice vector and Ω is the unit cell volume) by the Bloch functions through a Berry-phase expression, or alternatively, in real space through the charge centers of the Wannier functions [1,2]. It was also shown that the macroscopic surface charge of an insulating crystal is predicted by the standard bound-charge expression $\sigma^{\rm surf} = \mathbf{P}\cdot\hat{\mathbf{n}}$ (where $\hat{\mathbf{n}}$ is the surface normal) [3], as illustrated schematically in Fig. 1(a). The two-dimensional (2D) analog, the edge charge of a polar 2D insulating material, has been the subject of recent interest [4].

Here, we introduce and analyze a related quantity, the *surface polarization,* defined as a 2-vector $\boldsymbol{\mathcal{P}}$ lying in the plane of an insulating surface of an insulating crystal. By analogy with the bulk 3-vector $\boldsymbol{P}$, it has the property that when two facets meet, the linear bound-charge density appearing on the shared edge is predicted to be

$$\lambda^{\rm edge} = \boldsymbol{\mathcal{P}}_1\cdot\hat{\mathbf{n}}_1 + \boldsymbol{\mathcal{P}}_2\cdot\hat{\mathbf{n}}_2, \tag{1}$$

where $\boldsymbol{\mathcal{P}}_j$ is the surface polarization on facet j and $\hat{\mathbf{n}}_j$ is a unit vector lying in the plane of the facet and pointing toward (and normal to) the edge, as illustrated in Fig. 1(b).

This surface polarization $\boldsymbol{\mathcal{P}}$ is quite distinct from the dipole per unit area *normal* to the surface, which has also been called "surface polarization" by other authors [5,6]. The latter is always present regardless of the symmetry of the surface, and manifests itself macroscopically through the surface work function. In contrast, our surface polarization $\boldsymbol{\mathcal{P}}$ lies in plane and is nonzero only when the symmetry of the terminating surface supports a nonzero in-plane vector, as, for example, on the (110) surface of GaAs. It can also arise from a spontaneous symmetry-lowering surface reconstruction, as observed recently at the $Pb_{1-x}Sn_xSe$ (110) surface [7] and predicted for an ultrathin film of $SrCrO_3$ on (001) $SrTiO_3$ [8]. The surface polarization will be most evident when the bulk $\boldsymbol{P}$ vanishes, as will be the case for the systems discussed below.

The purpose of this Rapid Communication is to extend the Berry-phase theory to the case of surface polarization $\boldsymbol{\mathcal{P}}$ as defined above. To do this, we introduce a formulation based on hybrid Wannier functions (HWFs), which are Bloch-like parallel to the surface and Wannier-like in the surface-normal direction [9–12]. This allows for the use of Berry-phase methods parallel to the surface while allowing a real-space identification of the surface-specific contribution. We illustrate the concept first for a "toy" 2D tight-binding (TB) model, demonstrating the method of calculating the surface polarization. We then consider an atomistic three-dimensional (3D) model of an ideal (110) surface of a generic III-V zinc-blende semiconductor, using a TB model of GaAs to describe the electronic structure. In both cases, we confirm that the surface polarization correctly predicts corner and edge charges.

We first show how to express the surface polarization in terms of the Berry phases of HWFs for a 2D insulating sample, which we take to lie in the (x,z) plane. We take the "surface" (here really an edge) to be normal to $\hat{z}$ and introduce HWFs $|h_{lj}(k_x)\rangle$, where l indexes unit-cell layers normal to the z direction and j runs over occupied Wannier functions in a single unit cell. For the bulk, the lattice is periodic in z as well as x, and the $|h_{lj}(k_x)\rangle$ and their centers $z_{lj}^{\rm bulk}(k_x)$ can be obtained using the one-dimensional (1D) construction procedure given in Ref. [13]. To study the surface behavior we consider a ribbon consisting of a finite number of unit cells along $\hat{z}$. We then construct and diagonalize the matrix $Z_{mn} = \langle\psi_m(k_x)|z|\psi_n(k_x)\rangle$, whose eigenvectors yield the HWFs and whose eigenvalues give the HWF centers $z_{lj}(k_x)$. In practice, these are easily identified with the bulk $z_{lj}^{\rm bulk}(k_x)$ covering the range of l values that define the ribbon, with only modest shifts induced by the presence of the surface, allowing a common labeling scheme for both.

In order to calculate the polarization parallel to the surface, we compute the Berry phase

$$\gamma_{x,lj} = \int dk_x \langle h_{lj}|i\frac{d}{dk_x}|h_{lj}\rangle \tag{2}$$

of each HWF "band" (lj) as k_x runs across the 1D BZ. Doing the same for the bulk HWFs (these are independent of l) and taking the difference, we obtain a set of Berry-phase shifts $\Delta\gamma_{x,lj} \equiv \gamma_{x,lj} - \gamma_{x,j}^{\rm bulk}$ from which the electronic surface polarization can be determined via

$$\mathcal{P}_x^{\rm elec} = -\frac{ea}{\Omega\pi}\sum_{lj=\rm center}^{\rm top\ \ surf}\Delta\gamma_{x,lj}, \tag{3}$$

where a factor of 2 has been included for spin degeneracy and Ω is the edge repeat length a in 2D. Since $\Delta\gamma_{x,lj}$ decays exponentially into the bulk, the sum will converge within a few layers of the surface, but for definiteness we sum to the center of the ribbon. If the z_{lj} values of some neighboring HWF bands

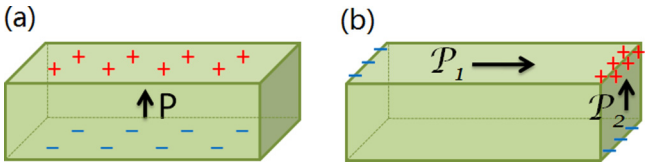

FIG. 1. (Color online) Illustration of bulk and surface polarization effects. The polarizations are denoted by black arrows, and net positive and negative bounded charged are in red and blue, respectively. (a) Bulk polarization gives rise to surface charges σ. (b) Surface polarization gives rise to edge charges λ.

overlap, the procedure needs to be generalized by grouping the HWFs into layers and using a multiband generalization to assign contributions to each layer.

The generalization to a 3D crystal with surface normal to z is straightforward. The HWFs are $|h_{lj}(k_x,k_y)\rangle$ with centers $z_{lj}(k_x,k_y)$. The surface polarization $\mathcal{P}_x^{\rm elec}$ is then obtained by computing Berry phases with respect to k_x as before, averaging over all k_y, and multiplying by the lattice constant a divided by the surface cell area Ω.

In the models considered in this Rapid Communication, the surface polarization is purely electronic, as the ions are held fixed in their bulk positions. More generally, $\mathcal{P}_x = \mathcal{P}_x^{\rm ion} + \mathcal{P}_x^{\rm elec}$ with the ionic contribution given by $\mathcal{P}_x^{\rm ion} = \Omega^{-1}\sum_{l\tau} Z_\tau (X_{l\tau} - X_{l\tau}^{\rm bulk})$, where Z_τ and $X_{l\tau}$ are the x position and bare charge of ion τ in cell l, and $X_\tau^{\rm bulk}$ is the corresponding bulk position of the same atom.

To illustrate these ideas, we start by considering a tight-binding (TB) model of the simple 2D crystal shown in Fig. 2(a). We assume a rectangular lattice with an aspect ratio $b/a = 0.8$. There are two atoms symmetrically located along a diagonal of the rectangular unit cell with coordinates $(\frac{1}{3},\frac{1}{3})$ and $(\frac{2}{3},\frac{2}{3})$, so that the bulk crystal has inversion symmetry. We consider only one s orbital per atom with on-site energy taken to be zero, and assume that each atom contributes one electron so that only the lower band is (doubly) occupied. We take the nonzero hoppings to be those shown in Fig. 2(a) and choose their values to be $t_1 = -2.2$, $t_2 = -0.15$, $t_3 = -0.1$, $t_4 = -0.09$, and $t_5 = -0.06$ in eV. The position operators are taken to be diagonal in the local-orbital representation so that $\langle\phi_i|z|\phi_j\rangle = z_i\delta_{ij}$.

We plot the bulk band structure of the TB Hamiltonian in Fig. 2(b). For the selected parameters the band gap is large compared to the bandwidths; in particular, the upper (unoccupied) band is quite flat. Next, we compute the surface polarization of a ribbon cut from the 2D lattice, taking it to be ten unit cells thick along z and infinite along x. We used an equally spaced 60-point k_x grid. At each k_x the 20×20 Hamiltonian is diagonalized, and the eigenfunctions $|\psi_n(k_x)\rangle$ are expressed in the tight-binding basis as $|\psi_n(k_x)\rangle = \sum_j c_{nj}(k_x)|\chi_j(k_x)\rangle$, where the $|\chi_j(k_x)\rangle$ are the Bloch basis function formed as a Fourier sum at wave vector k_x of atomic orbitals $|\phi_i\rangle$. From the ten occupied bands we construct the 10×10 position matrix $Z_{mn} = \langle\psi_m(k_x)|z|\psi_n(k_x)\rangle = \sum_j z_j c_{mj}^*(k_x)c_{nj}(k_x)$. Diagonalizing this matrix, we get ten eigenvalues $z_l(k_x)$ that can each be clearly associated with a particular unit cell layer, and ten eigenfunctions that are the HWFs. We label the HWF $|h_l(k_x)\rangle$, where l is the layer index running from the bottom to the top of the ribbon.

Next we calculate $\gamma_{x,l}$, the Berry phase along k_x, for each l using Eq. (2). Deep in the interior these Berry phases become equal to π within numerical precision, while the Berry phases near the edge are slightly shifted away from π, leading to a nonzero surface polarization as shown in Fig. 2(c).

The value of the surface polarization obtained from Eq. (3) is $\mathcal{P}_x = \pm2.1\times10^{-4}e$ for the top and bottom surfaces, respectively. Similarly, we can compute the surface polarizations for the left/right surfaces using a ribbon ten cells wide in x and infinite along z. We obtain $\mathcal{P}_z = \pm4.7\times10^{-4}e$ along the left and right edges, respectively. At the corners, the surface polarizations are directed head to head or tail to tail, as shown in Fig. 2(a).

We then predict that the charge accumulation at the corner of a finite sample should equal the sum of the two adjacent surface polarizations, here $|\mathcal{P}_x| + |\mathcal{P}_z| = 6.8\times10^{-4}e$. To test this, we directly calculate the corner charge in a finite 2D sample, specifically a 10×10 supercell, large enough to ensure neutrality in the central region and in the middle of the edges of the sample. The corner charge is obtained by summing up the on-site charge differences, relative to the bulk, for atoms in the quadrant containing the corner. We find $Q_{\rm corner} = \pm6.8\times10^{-4}e$, in agreement with our prediction from the computed surface polarizations.

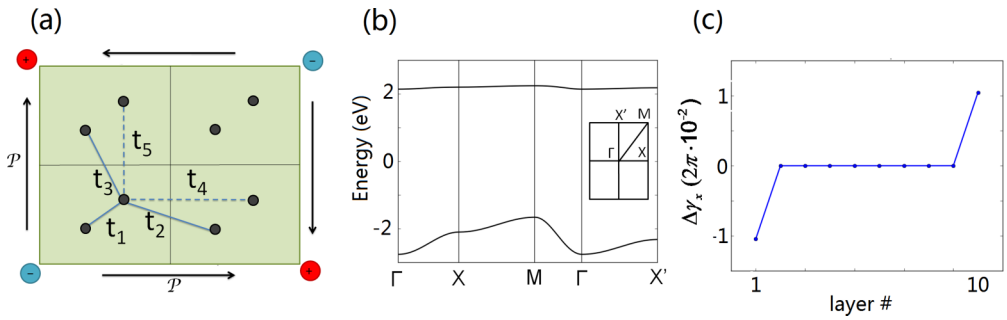

FIG. 2. (Color online) (a) Illustration of the TB model, where four unit cells are presented. The atoms are denoted by black dots. Nearest-neighbor hoppings t_1, t_2, and t_3 are shown as solid blue lines. Next-nearest-neighbor hoppings t_4 and t_5 are shown as dashed blue lines. $\mathcal{P}$ are shown by black arrows. The induced $Q_{\rm corner}$ are denoted by red (positive) and blue (negative) large dots at the corners. (b) Band structure of the TB model in the (k_x,k_z) space. The inset shows the high symmetry points in the 2D Brillouin zone, where Γ, X, M, X' refer to (0,0), $(0,\frac{1}{2})$, $(\frac{1}{2},\frac{1}{2})$, and $(\frac{1}{2},0)$, respectively. (c) Difference between effective x positions of each HWF and that deep in the bulk.

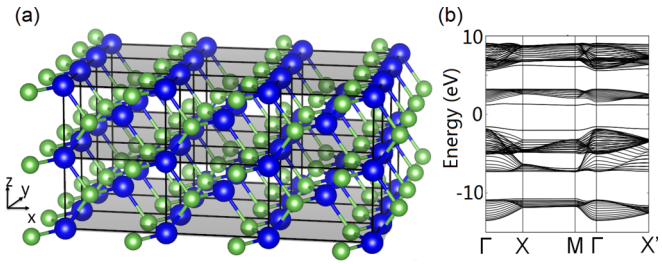

FIG. 3. (Color online) (a) Illustration of the GaAs slab studied in the TB model, where the blue and green balls represent Ga and As atoms, respectively. The gray shaded planes denote the (110) family planes. (b) Electronic band structure of the GaAs slab in the 2D Brillouin zone, with the thickness of eight cells z.

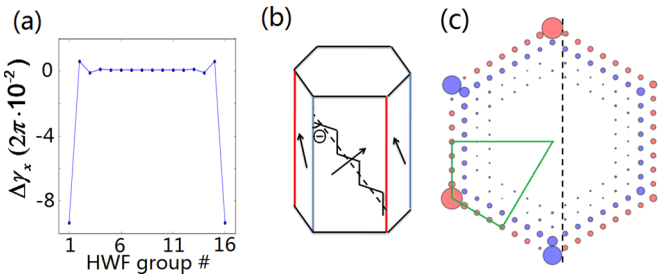

FIG. 4. (Color online) (a) Difference between the γ_x of each group of HWFs and that deep in the bulk. (b) Overhead view of the hexagonal GaAs nanowire. The dashed black line, which meets the edges along [111] at an angle of $\theta = 35.26°$, shows the direction along which the zigzag surface chains run. The relevant surface polarizations at the side surfaces are denoted by black arrows. The blue and red vertical edges mean net negative and positive edge charge distributions, respectively. (c) On-site charge distribution summed over the trilayer. Red and blue dots represent positive and negative net charges, respectively. The sizes of the dots indicate the magnitudes of the on-site net charge. The left and right regions to the dashed vertical line show the total and symmetric part of on-site charges, respectively.

We now consider a TB model of a generic III-V zinc-blende semiconductor, with GaAs as the prototypical example. The crystal structure is characterized by Ga-As zigzag chains running along $\langle 110 \rangle$. Although the crystal structure does not have inversion symmetry, the tetrahedral symmetry forbids a nonzero spontaneous polarization. We use tight-binding parameters from Ref. [14], in which is shown the bulk band structure and density of states. The unit cell contains two Ga and two As atoms, each with four sp^3 hybridized orbitals and four electrons, as shown in Fig. 3(a). The position matrix is assumed to be diagonal and atom centered in the basis of tight-binding orbitals [15].

To describe the (110) surface, we construct a slab geometry as shown in Fig. 3(a), and we henceforth label the Cartesian directions as shown there. That is, the surface, which is normal to $\hat{z}$, has zigzag chains running along $\hat{y}$. Since the two atoms making up these chains are inequivalent, we expect a surface polarization in the $\hat{x}$ direction. We take the slab to be eight unit cells thick; for the atoms in the surface layer, the hoppings to the atoms inside the slab are the same as in the bulk, while the hoppings to the vacuum side are set to zero. At each (k_x,k_y) of the 100×100 k grid in the surface BZ, the 128×128 Hamiltonian is diagonalized, and we obtain the band structure for the slab, shown in Fig. 3(b). Surface states are evident as isolated bands.

Next, we diagonalize the 64×64 position matrices $Z(k_x,k_y)$ constructed from the eigenstates of the occupied bands. The eigenvalues, which are the z coordinates of the HWF centers, can be clearly divided into groups, each consisting of four HWFs j representing the four Ga-As bonds around an As atom, each group being associated with one of the 16 atomic layers l. In this case, it is more useful to calculate the Berry phase of each group of HWFs rather than of each single HWF [3].

As expected, the Berry phase in the $\hat{y}$ direction along the zigzag chain is found to be zero, but in the $\hat{x}$ direction it is nonzero for the HWF groups near the top and bottom surfaces of the slab. Thus, we confirm that there is a nonzero surface polarization $\mathcal{P}_x$. We plot the difference between the Berry phase γ_x of each group of HWFs and that for the bulk in Fig. 4(a). By summing up the contributions from each group of HWFs from the center of the bulk to one surface, the total surface polarization is found to be $0.178e/L$. Here, $L = a/\sqrt{2}$ is the repeat length of the zigzag chain, i.e., the surface cell dimension along $\hat{y}$, where a is the surface lattice constant along $\hat{x}$. Subdividing the dominant surface-group contribution further, we find that the surface polarization comes mainly from the surface-most HWF, corresponding to a shift of the center of the dangling bond on the surface As atom.

The surface polarization on the {110} surfaces predicts an accumulated line charge for the common edge of two such surfaces. In order to demonstrate this effect, we consider a hexagonal wire of GaAs that is infinite along [111], with a periodicity corresponding to three of the GaAs buckled (111) layers. In this case, the six side surfaces of the wire are all {110} planes. As shown in Fig. 4(b), on each side facet the surface polarization is perpendicular to the zigzag chains, forming a pattern of $\boldsymbol{\mathcal{P}}$ vectors shown as black arrows. The surface polarizations for each neighboring pair of side facets have a common component along [111], but are head to head or tail to tail for the component normal to [111], leading to alternating positive and negative line charges for the six edges as shown. According to Eq. (1), we expect the line charge per three-layer vertical period to be $Q_{3L} = (2\mathcal{P}\cos\theta)(3L\cos\theta) = 0.71e$, where the $3L\cos\theta$ factor is the vertical period.

For comparison, we directly calculate the edge charges per trilayer period in a nanowire with a radius of eight atoms. We sum up the site populations within the TB model with a 60-point k grid along [111]. The on-site charge is the difference from the bulk value. The computed on-site charges are shown in the left half of Fig. 4(c), while the right half shows the corresponding results after averaging with a 60°-rotated version of itself. The surface charges decay rapidly into the bulk, leading to a neutral bulk state inside the nanowire. Also, a surface dipole density normal to the surface is clearly visible, especially in the orientationally averaged results. However, we are interested in the accumulation at the edges, which is obviously present in the unaveraged results in the left half of the figure. The edge charge is calculated by summing up

the on-site charges in the wedge-shaped region illustrated in Fig. 4(c), using a weight of 1/2 for atoms located on its radial edges. The total edge charge per trilayer is found to be $\pm 0.71e$, in agreement with the value predicted using the previously calculated surface polarization.

We emphasize that this numerical value is not intended to be realistic for GaAs. A more accurate estimate would require the use of an improved tight-binding model and treatment of surface relaxations and dielectric screening effects. Our purpose here has been to show that the surface polarization as defined here correctly predicts edge charges. We note that an analysis based on maximally localized Wannier functions [16] is also possible. However, we believe our HWF-based approach is more natural, as the Wannier transformation is only done in the needed direction and no iterative construction is required.

We stress that the concept of surface polarization $\mathcal{P}$ is quite general, occurring whenever the surface symmetry is low enough. In some cases this can arise from a spontaneous symmetry-lowering surface relaxation or reconstruction, allowing "surface ferroelectricity" if it is switchable. In other cases, as for GaAs (110), the ideal surface space group already has low enough symmetry to allow a nonzero $\mathcal{P}$. This will occur quite generally for low-angle vicinal surfaces. The concept also applies to planar defects such as domain walls, stacking faults, and twin boundaries, and to heterointerfaces; if $\mathcal{P}$ is present within this plane, it may induce a line charge where the plane intersects the surface. Such edge and line charges are potentially observable using electric force microscopy [17], electron holography [18], or other experimental methods. Another possibility is to use scanning tunneling microscopy to observe the point defects or ionic adsorbates that may be attracted by the line charge. Finally, we note that the concept of surface polarization may become more subtle in the presence of orbital magnetization, which we have omitted from our considerations here.

In summary, we have formulated the concept of surface polarization, i.e., the dipole moment per unit area *parallel* to the surface, which can exist whenever the surface symmetry is low enough. Using TB models we have computed the surface polarizations for a 2D toy model and a generic III-V zinc-blende semiconductor, and shown that the predicted corner or edge charges are in good agreement with direct calculations. We point out that surface and interface polarizations can be responsible for observable effects, and perhaps even desirable functionality, in a broad range of insulating materials systems.

We acknowledge helpful discussions with Hongbin Zhang, Jianpeng Liu, and Massimiliano Stengel. This work is supported by National Science Foundation DMR-14-08838 and Office of Naval Research N00014-11-1-0665.

[1] R. D. King-Smith and D. Vanderbilt, Phys. Rev. B **47**, 1651 (1993).
[2] R. Resta, Rev. Mod. Phys. **66**, 899 (1994).
[3] D. Vanderbilt and R. D. King-Smith, Phys. Rev. B **48**, 4442 (1993).
[4] M. Gibertini, G. Pizzi, and N. Marzari, Nat. Commun. **5**, 5157 (2014).
[5] L. Bányai, P. Gilliot, Y. Z. Hu, and S. W. Koch, Phys. Rev. B **45**, 14136 (1992).
[6] W. Wen, X. Huang, S. Yang, K. Lu, and P. Sheng, Nat. Mater. **2**, 727 (2003).
[7] Y. Okada, M. Serbyn, H. Lin, D. Walkup, W. Zhou, C. Dhital, M. Neupane, S. Xu, Y. J. Wang, R. Sankar, F. Chou, A. Bansil, M. Z. Hasan, S. D. Wilson, L. Fu, and V. Madhavan, Science **341**, 1496 (2013).
[8] K. Gupta, P. Mahadevan, P. Mavropoulos, and M. Ležaić, Phys. Rev. Lett. **111**, 077601 (2013).
[9] C. Sgiarovello, M. Peressi, and R. Resta, Phys. Rev. B **64**, 115202 (2001).
[10] X. Wu, O. Diéguez, K. M. Rabe, and D. Vanderbilt, Phys. Rev. Lett. **97**, 107602 (2006).
[11] A. A. Soluyanov and D. Vanderbilt, Phys. Rev. B **83**, 235401 (2011).
[12] M. Taherinejad, K. F. Garrity, and D. Vanderbilt, Phys. Rev. B **89**, 115102 (2014).
[13] N. Marzari and D. Vanderbilt, Phys. Rev. B **56**, 12847 (1997).
[14] J. D. Joannopoulos and M. L. Cohen, Phys. Rev. B **10**, 5075 (1974).
[15] J. Bennetto and D. Vanderbilt, Phys. Rev. B **53**, 15417 (1996).
[16] N. Marzari, A. A. Mostofi, J. R. Yates, I. Souza, and D. Vanderbilt, Rev. Mod. Phys. **84**, 1419 (2012).
[17] G. Valdrè, Imaging Microsc. **8**, 44 (2006).
[18] D. Wolf, H. Lichte, G. Pozzi, P. Prete, and N. Lovergine, Appl. Phys. Lett. **98**, 264103 (2011).